

Received July 6, 2020, accepted July 15, 2020, date of publication July 28, 2020, date of current version August 19, 2020.

Digital Object Identifier 10.1109/ACCESS.2020.3012559

# Intelligent Fault Diagnosis of Rolling Bearing Using FCM Clustering of EMD-PWVD Vibration Images

HONGWEI FAN<sup>1,2</sup>, SIJIE SHAO<sup>1</sup>, XUHUI ZHANG<sup>1,2</sup>, (Member, IEEE),

XIANG WAN<sup>1,2</sup>, XIANGANG CAO<sup>1,2</sup>, AND HONGWEI MA<sup>1,2</sup>

<sup>1</sup>School of Mechanical Engineering, Xi'an University of Science and Technology, Xi'an 710054, China

<sup>2</sup>Shaanxi Key Laboratory of Mine Electromechanical Equipment Intelligent Monitoring, Xi'an 710054, China

Corresponding author: Hongwei Fan (hw\_fan@xust.edu.cn)

This work was supported in part by the National Natural Science Foundation of China under Grant 51605380, in part by the Natural Science Basic Research Project of Shaanxi Province in China under Grant 2019JLZ-08, and in part by the Key Research and Development Project of Shaanxi Province in China under Grant 2019GY-093.

**ABSTRACT** Rolling bearing is key component of rotating machinery and its fault diagnosis is of great significance for reliable operation of machine. In this paper, an intelligent fault diagnosis method of rolling bearing based on FCM clustering of vibration images obtained by EMD-PWVD is presented. Firstly, vibration signals with different fault degrees are transformed into contour time-frequency images by EMD-PWVD. Secondly, vibration images are divided into sections and their energy distribution values are used as image feature. Then, feature vectors are constructed for known signals, which are standardized as inputs of FCM clustering to obtain classification matrix and clustering center. Finally, proximity between tested samples and clustering centers of known samples are calculated to realize identification of bearing faults. Experimental results show that identification accuracy of this proposed method is high. When adding noise, the proposed method is more stable than other vibration images such as grayscale and symmetrical polar coordinate image, and when the added noise with SNR of 5, the reduction rate of identification accuracy is obviously smaller than those of other two methods.

**INDEX TERMS** Rolling bearing, fault diagnosis, vibration image, empirical mode decomposition (EMD), pseudo-Wigner-Ville distribution (PWVD), fuzzy C-means (FCM) clustering.

## I. INTRODUCTION

Rolling bearing is key component of rotating machinery, which has characteristics of high speed, complex structure and easy fault in operation. Defects and damages of rolling bearing directly affect performance and life of entire rotating machine, therefore its fault diagnosis is of great practical significance [1].

Vibration signal analysis is usually used for fault diagnosis of rolling bearing, including time-domain, frequency-domain and time-frequency analysis (TFA). Time-domain analysis includes waveform analysis, correlation analysis, kurtosis analysis and so on [2]–[4]. Frequency-domain analysis includes Fourier transform, envelope demodulation, cepstrum analysis and so on [5]–[8]. Since fault-induced vibration

signal of rolling bearing is non-linear and non-stationary and early weak fault signal is often drowned in strong background noise, so conventional time-domain and frequency-domain analysis are often difficult to accurately extract fault information. TFA can simultaneously reproduce time-domain and frequency-domain features of signal, which is very effective for nonlinear and non-stationary signal, so TFA is widely used for fault diagnosis of rolling bearing. TFA mainly includes two basic kinds of wavelet transform and empirical mode decomposition (EMD). Wavelet transform [9], [10] can suppress white noise effectively and EMD [11] has better adaptability. Kumar and Singh [12] used wavelet analysis to extract shock information from fault-induced vibration signal of tapered roller bearing and error was controlled in a small range. Liu *et al.* [13] proposed synchronous compression wavelet transform, which has higher feature extraction precision and time-frequency resolution. Guo and Deng [14]

The associate editor coordinating the review of this manuscript and approving it for publication was Yue Zhang<sup>1</sup>.

proposed optimization algorithm-based EMD, which effectively extracted fault characteristics of bearing ring. Rezaee and Osguei [15] proposed local mean method to eliminate modal mixing and endpoint effects of EMD. In addition to wavelet analysis and EMD, Wigner-Ville distribution (WVD) [16] is also an important quadratic TFA method, which has high time-frequency resolution, but it has cross term [17], which can not be directly used for TFA. Cai *et al.* [18] and Mu *et al.* [19] proposed TFA method combining EMD with WVD, which not only effectively restrains cross term, but also guarantees time-frequency aggregation. In order to get rid of cross term, WVD adding time-domain window function was also proposed, i.e., pseudo-Wigner-Ville distribution (PWVD) [20], [21].

Due to intuitiveness of image, typical image analysis methods such as grayscale image (GI) and symmetrical polar coordinate image (SPCI) are paid attention besides TFA. Uddin *et al.* [22] used GI through Gabor filtering to realize noise reduction and feature extraction of engine, and Liu *et al.* [23] used GI texture analysis-based fault feature extraction to reduce noise and identify fault of engine. Time-domain signal is transformed into polar coordinate image by Jia *et al.* [24] to implement visual fault identification of mechanical transmission, and filtered signal is transformed into image using SPCI method by Yang and Feng [25] to carry out visual diagnosis of internal combustion engine.

With development of artificial intelligence, fault diagnosis is more and more introduced into new pattern recognition. After extracting fault features, pattern recognition is needed to realize intelligent diagnosis, most widely used identification methods are artificial neural network [26], [27], support vector machine [28], [29] and clustering algorithm [30], [31]. Among them, clustering is simple. Fuzzy C-means (FCM) clustering is more flexible than hard clustering. Zhou *et al.* [32] combined EMD and singular value decomposition with FCM clustering to achieve fault identification of rolling bearing. Ren *et al.* [33] and Zhang *et al.* [34] transformed vibration signal into mirror symmetry snowflake image using SPCI and extracted image features, then FCM clustering was used to realize fault identification.

To sum up, combining vibration image with pattern recognition can realize intelligent fault diagnosis of rolling bearing intuitively. However, there is still no research on the intelligent diagnosis combining EMD-PWVD and FCM clustering for rolling bearings. Therefore, based on time-frequency characteristics of EMD and PWVD and merits of FCM clustering, this paper presents a new vibration image clustering method of EMD-PWVD-FCM to diagnose fault of rolling bearing. In Section 1, principle of EMD-PWVD, image generation and feature extraction are introduced. Section 2 gives principle of FCM clustering. Feature extraction of GI and SPCI are introduced in Section 3. And in final Section, EMD-PWVD, GI and SPCI are compared to prove effectiveness and robustness of the proposed method combining EMD-PWVD with FCM clustering.

## II. EMD-PWVD-BASED TFA METHOD

### A. BASIC PRINCIPLE

#### 1) BASIC THEORY OF EMD

EMD decomposes vibration signal into a series of independent intrinsic mode functions (IMFs) with different characteristic time scales, each IMF is a single component signal. For any signal  $x(t)$ , firstly we determine all extreme points of  $x(t)$ , and then upper and lower envelopes are obtained by third-order spline interpolation. Let  $m(t)$  be average of upper and lower envelopes and  $h(t)$  be difference between  $x(t)$  and  $m(t)$ , then there are

$$m(t) = [x_{\max}(t) + x_{\min}(t)]/2 \quad (1)$$

$$h(t) = x(t) - m(t) \quad (2)$$

Treat  $h(t)$  as new  $x(t)$ , and repeat above operations until  $h(t)$  meets a certain criteria, for example, change of  $h(t)$  before and after repeating operations is small enough, mark  $imf_1 = h(t)$ , where  $imf_1$  is an IMF, and then make

$$r_1(t) = x(t) - imf_1 \quad (3)$$

Think of  $r_1(t)$  as new  $x(t)$ , repeat process to get the second IMF, third IMF, and so on. When  $imf_n$  or  $r_n(t)$  satisfies given stopping condition, for example, IMF or  $r_n(t)$  is small enough or  $r_n(t)$  is monotone function, the above process terminates to obtain decomposition formula

$$x(t) = \sum_{i=1}^n imf_i + r_n(t) \quad (4)$$

where  $r_n(t)$  is residual function and represents average trend of signal.

#### 2) BASIC THEORY OF PWVD

WVD is a kind of bilinear time-frequency distribution, which is defined as Fourier transform of center covariance function of signal. For continuous signals in time domain, WVD is

$$W_x(t, f) = \int_{-\infty}^{\infty} x(t + \frac{\tau}{2})x^*(t - \frac{\tau}{2})e^{-j2\pi f\tau} d\tau \quad (5)$$

where  $t$  is time-domain variable,  $f$  is frequency-domain variable, and  $x^*(t - \frac{\tau}{2})$  is conjugate transpose of  $x(t + \frac{\tau}{2})$ .

For signal  $x(t) = x_1(t) + x_2(t)$ , WVD is

$$W_x(t, f) = W_{x_1}(t, f) + W_{x_2}(t, f) + 2Re[W_{x_1, x_2}(t, f)] \quad (6)$$

where

$$W_{x_1, x_2}(t, f) = \int_{-\infty}^{+\infty} x_1(t + \frac{\tau}{2})x_2^*(t - \frac{\tau}{2})e^{-j2\pi f\tau} d\tau \quad (7)$$

It can be seen that WVD of sum of two signals is not equal to sum of their respective WVDs, and there exists cross term  $2Re[W_{x_1, x_2}(t, f)]$ . More signal components, more cross-terms. If signal contains  $n$  components, it will produce  $n(n-1)/2$  cross-terms. Existence of cross terms leads to false signal and false frequency, which makes WVD difficult to clearly express signals with multiple frequency components.

In order to solve problem of cross terms, WVD is windowed to obtain PWVD, which is defined as follows

$$PW_x(t, f) = \int_{-\infty}^{\infty} h(\tau)x(t + \frac{\tau}{2})x^*(t - \frac{\tau}{2})e^{-j2\pi f\tau} d\tau \quad (8)$$

where  $h(\tau)$  is window function.

### 3) BASIC THEORY OF EMD-PWVD

Since PWVD can only solve the time domain problem, EMD-PWVD is proposed in this paper. EMD-PWVD of signal  $x(t)$  is defined as

$$EMD\_PW_x(t, f) = \sum_{i=1}^n \frac{\int_{-\infty}^{\infty} fPW_{IMF_i}(t, f)}{PW_{IMF_i}(t, f)} \quad (9)$$

where, EMD-PWVD decomposes multi-component signals into single component and finite sum of IMFs, then PWVD is performed on each IMF, then PWVD results of different IMFs are superimposed to obtain time-frequency distribution of vibration signals. Combination of EMD and PWVD not only effectively eliminates cross terms of WVD, but also retains original time-frequency focusing of WVD.

### B. IMAGE GENERATION

Fig. 1 is 3D EMD-PWVD time-frequency distribution of vibration signals of normal rolling bearing at 1797r/min, it is a joint function of time and frequency and describes energy intensity of signals at different times and frequencies, thus, time-frequency characteristics of signals is directly expressed. Fig. 2 is 2D contour time-frequency map, it also describes energy intensity of signals at different times and frequencies. Contour map shown in Fig. 2 is projection of 3D plot shown in Fig. 1 in time-frequency plane, and information expressed in these two plots is the same. In order to express more simply, contour map is used in this paper.

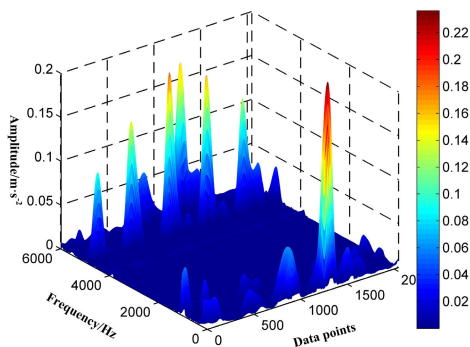


FIGURE 1. 3D time-frequency plot.

Because 2D contour map can reflect energy distribution of vibration signals in different times and frequencies, so it is different for different fault states of rolling bearing.

### C. FEATURE EXTRACTION

A group of vibration data at 1797r/min from rolling bearing with normal state and inner ring defects of 0.007 and

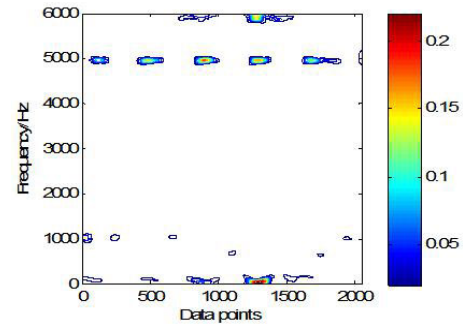


FIGURE 2. 2D time-frequency contour map.

0.021 inches are shown in Fig. 3, EMD-PWVD method was used to obtain time-frequency images of three vibration signals. Results are shown in Fig. 4.

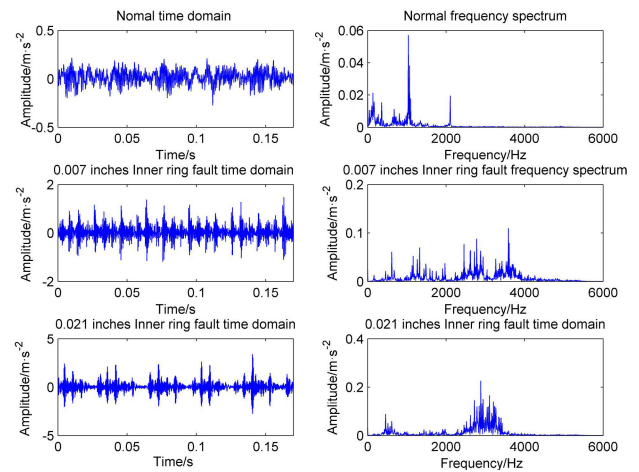


FIGURE 3. Time-domain waveform and frequency-domain spectrum diagram under normal and two fault cases.

As can be seen from Fig. 4, energy distribution in three states is different. Fig. 4(a) is time-frequency map of normal bearing, and its energy distribution is mainly in 4-6KHz, there are also a few in 0-2KHz. Fig. 4(b) is time-frequency map of bearing with defect of 0.007 inches, energy distribution is mainly in 2-4KHz, there are also a few in 0-2KHz and 4-6KHz. Fig. 4(c) is time-frequency map of bearing with defect of 0.021 inches, and energy distribution is mainly in 2-4KHz. Therefore, according to characteristics of energy distribution, vibration data are divided into three energy intervals: 0-2KHz, 2-4KHz and 4-6KHz, as shown in Fig. 4, contour map is divided into different sections, and fault state can be identified according to accumulated energy value of each section.

When intervals are divided more, identification accuracy is higher, but identification complexity will increase and efficiency will decrease. As can be seen from Table 1, energy distribution values at three frequency ranges are obviously different, so energy values in three intervals were chosen as characteristic parameters of fault identification.

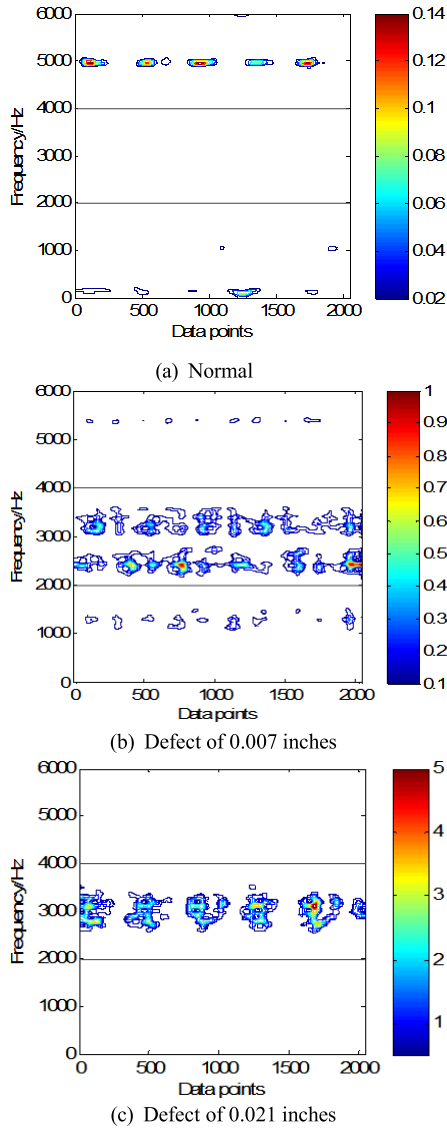


FIGURE 4. Energy partition diagrams of contour time-frequency maps under different states.

TABLE 1. Accumulated energy values of rolling bearing under different states.

State of rolling bearing	0-2KHz accumulated energy	2-4KHz accumulated energy	4-6KHz accumulated energy
Normal	0.0017	3.5580E-05	0.0054
Inner ring fault diameter of 0.007 inches	0.0161	0.0661	0.0090
Inner ring fault diameter of 0.021 inches	0.0057	0.2251	0.0257

### III. FCM CLUSTERING METHOD

#### A. ALGORITHM MODEL

FCM clustering algorithm is a soft clustering algorithm based on objective function, which has characteristics of rigorous

theory and good clustering effect. FCM optimizes objective function to get membership degree of each sample point to all class centers, and then determines class attributes of sample points, so as to automatically group samples with similar characteristics into one class [35].

Suppose we know initial membership degree matrix  $U = [u_{ij}]_{c \times n}$  and clustering center matrix  $C = [c_1, c_2, \dots, c_c]^T$  of data set vector  $X = \{x_1, x_2, \dots, x_n\}$ , where  $u_{ij}$  is membership degree of  $x_j$  relative to  $c_i$ , and  $u_{ij}$  satisfies

$$0 \leq u_{ij} \leq 1 \quad (10)$$

$$\sum_{i=1}^c u_{ij} = 1 \quad (11)$$

$$\sum_{j=1}^n u_{ij} > 1 \quad (12)$$

where  $0 \leq i \leq c$ ,  $1 \leq j \leq n$ ,  $c$  is number of classification, i.e., number of clustering centers, and  $n$  is number of samples. Essence of FCM clustering is iterative convergence process of objective function by updating clustering center matrix  $C$  and membership degree matrix  $U$  [36].

Objective function of FCM clustering is defined as

$$J_{fcm}(U, C) = \sum_{j=1}^n \sum_{i=1}^c u_{ij}^m d_{ij}^2 \quad (13)$$

where  $m$  is fuzzy weighted index, usually  $m = 2$ ,  $d_{ij}$  is Euclidean distance from sample point  $x_j$  to center  $c_i$ , i.e.,

$$d_{ij} = \|x_j - c_i\| = (x_j - c_i)^T (x_j - c_i) \quad (14)$$

Steps of FCM clustering are as follows.

Step 1: determine number of clustering centers  $c$ , number of iterations  $l = 0$ , and initialize classification matrix  $U = [u_{ij}]_{c \times n}$ .

Step 2: calculate membership degree matrix  $U$ .

$$u_{ij} = 1 / \sum_{i=1}^c \left( \frac{d_{ij}}{d_{kj}} \right)^m \quad (15)$$

Step 3: update clustering center matrix  $C$ .

$$c_i = \sum_{j=1}^n u_{ij}^m x_j / \sum_{j=1}^n u_{ij}^m \quad (16)$$

Take appropriate norm  $\varepsilon > 0$ , terminate operation if  $\|U^{l+1} - U^l\| < \varepsilon$  is satisfied, otherwise  $l = l + 1$ , repeat above steps 2 and 3 until condition is satisfied.

#### B. CLUSTERING SCHEME

In this paper, near selection principle is used for fault clustering [34]. Set standard mode  $S_i (i = 1, 2, \dots, n)$  and object  $T$  to be identified as two fuzzy subsets, if  $i_0$  exists, make

$$N(S_{i_0}, T) = \max\{N(S_1, T), N(S_2, T), \dots, N(S_n, T)\} \quad (17)$$

then  $T$  and  $S_{i_0}$  are considered to be closest, and they are judged to be of the same class.

Degree of closeness is calculated using Hamming degree of closeness, and its expression is

$$N(S, T) = 1 - \frac{1}{n} \sum_{k=1}^n |S(x_k) - T(x_k)| \quad (18)$$

The greater the closeness  $N(S, T)$  is, the more similar the two patterns are, and vice versa. This approach can ensure that samples to be identified are effectively classified to  $c$  categories, and achieve reasonable classification of all data.

#### IV. VIBRATION IMAGE TRANSFORM METHOD COMPARED WITH EMD-PWVD

In order to prove advantages of the proposed EMD-PWVD method, two vibration image transform methods of GI and SPCI were used to compare with EMD-PWVD.

##### A. GI ANALYSIS

Transforming vibration signal into GI can not only reflects intrinsic characteristics of signal, but also analyzes relationship between adjacent sampling points. GI analysis is to transform vibration signal into 2D grayscale image to extract local features using local binary patterns (LBP) algorithm, and then identify characteristic frequency by 2D Fourier transform.

##### 1) IMAGE GENERATION

Steps of transforming vibration signal into GI are as follows. Step 1: standardize amplitude of each sampling point of vibration signal, and distribute it in value range of image pixels, i.e., 0-255.

Step 2: divide vibration signal into  $N$  sub-regions, each interval contains  $M$  sampling points, and values of  $M$  and  $N$  depend on total number of sampling points of signals.

Step 3: amplitude of each sub-interval sampling point is taken as grayscale value of each point at each line, realize vibration signal into GI.

As shown in Fig. 5, the smaller the values of  $M$  and  $N$ , the simpler the calculation, to ensure that useful information can be retained for original signal, usually  $M$  and  $N$  are 128, 256 or 512.

##### 2) LBP-BASED GI TEXTURE ANALYSIS

LBP is an image texture feature extraction algorithm. Texture feature of image pixel is relationship between current pixel and its surrounding pixels. LBP has advantages of rotational invariance and grayscale level invariance [37]. Example of LBP operator is shown in Fig. 6.

As shown in Fig. 6, in window of  $3 \times 3$ , grayscale values of 8 adjacent pixels are compared with threshold value of center pixel in window. If values of surrounding pixels are larger than that of center pixel, position of this pixel point is marked as 1, otherwise 0. In this way, 8-bit binary number was generated by comparing 8 points in  $3 \times 3$  neighborhood, which is converted to decimal number, i.e., LBP code, so 256 LBP numbers are obtained. LBP value of pixel point in center of

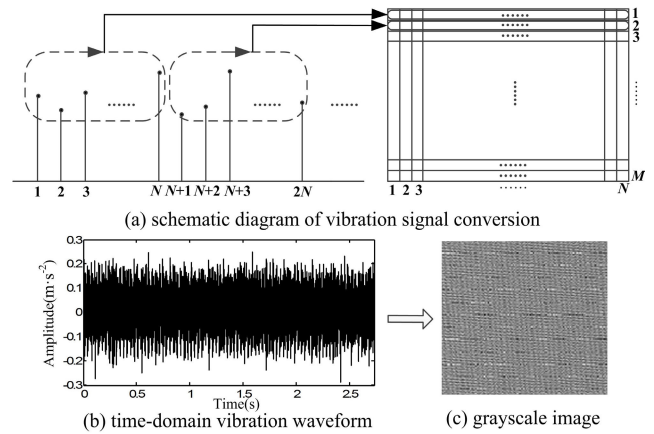


FIGURE 5. Schematic diagram of transformation from vibration signal to gray image.

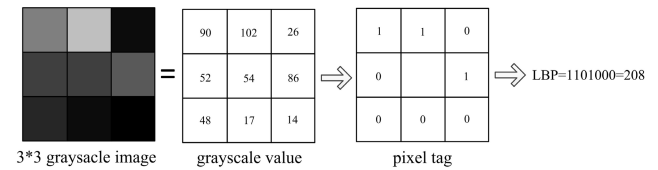


FIGURE 6. Illustration of LBP operator.

window is used to reflect texture information of this area.

$$LBP(x_c, y_c) = \sum_{p=0}^{p-1} 2^p S(i_p - i_c) \quad (19)$$

where  $(x_c, y_c)$  represents  $3 \times 3$  neighborhood center element, its pixel value is  $i_c$ ,  $i_p$  represents other pixel values in neighborhood,  $p$  is pixel numbers at neighborhood center, and  $S(x)$  is a symbolic function defined as follows

$$S(x) = \begin{cases} 1, & x \geq 0 \\ 0, & x < 0 \end{cases} \quad (20)$$

##### 3) 2D FOURIER TRANSFORM OF GI

2D Fourier transform (2D-FT) is a commonly used image processing method, which is of great value for image enhancement, denoising, edge detection and so on [38]. 2D-FT transforms image from spatial domain to frequency domain, transforming image's grayscale distribution function into frequency distribution function. Let  $f(x, y)$  represent GI of  $M \times N$ , where  $x = 0, 1, \dots, M-1, y=0, 1, \dots, N-1$ , 2D discrete Fourier transform is

$$f(u, v) = \frac{1}{MN} \sum_{x=0}^{M-1} \sum_{y=0}^{N-1} f(x, y) e^{-j2\pi ux/M} e^{-j2\pi vy/N} \quad (21)$$

where  $u = 0, 1, \dots, M-1, v = 0, 1, \dots, N-1$ , and 2D-FT has shift property in space, i.e.,

$$f(x - a, y - b) \Leftrightarrow F(u, v) e^{-j2\pi(aux/M + bv/N)} \quad (22)$$

In 2D-FT, we can see bright and dark spots, which express difference between a point and its neighbors, i.e., gradient

size, or frequency size of point. Frequency of image is index of intensity of image grayscale. If gradient is large, intensity of point is strong, and vice versa. Gradient gives direct view of energy distribution of image. Shift in space domain of image causes phase change in frequency domain. When the frequency of frequency spectrum is moved to center of circle, frequency distribution of image is clearly seen and periodic interference signals are separated, thus, fault feature in original vibration signal can be extracted effectively.

In order to quantify brightness of 2D-FT image, according to properties of grayscale image, square sum of matrix elements for 2D-FT image is calculated, and total brightness  $E$  of image is quantitatively evaluated according to calculated results [39].

$$E = \sum_{i=1}^n x_i^2 \tag{23}$$

where  $x$  is matrix element value of GI,  $n$  is total number of sampling points, i.e., total number of matrix elements.

**B. SPCI ANALYSIS**

SPCI method [34] makes vibration signal transform directly from time domain waveform to image without TFA. Vibration signal is transformed into 2D image, and image feature is extracted by gray level co-occurrence matrix (GLCM) [40].

**1) IMAGE GENERATION**

Schematic diagram of SPCI method is shown in Fig. 7. In Fig. 7,  $\gamma(i)$  is polar coordinate radius,  $\alpha(i)$  and  $\beta(i)$  are counterclockwise and clockwise rotation angles from initial line. In discrete sampling data sequence of vibration signal, vibration parameter at time  $i$  is assumed to be  $x_i$ , and that at time  $i + \Delta\tau$  is assumed to be  $x_{i+\Delta\tau}$ , bringing into Eq. (24) to Eq. (26), converting into a point  $P(\gamma(i), \alpha(i), \beta(i))$  in polar coordinate space, by changing rotation angle, vibration signal forms mirror-symmetrical image.

$$\gamma(i) = \frac{x_i - x_{\min}}{x_{\max} - x_{\min}} \tag{24}$$

$$\alpha(i) = \phi + \frac{x_{i+\Delta\tau} - x_{\min}}{x_{\max} - x_{\min}} k \tag{25}$$

$$\beta(i) = \phi - \frac{x_{i+\Delta\tau} - x_{\min}}{x_{\max} - x_{\min}} k \tag{26}$$

where  $x_{\max}$  is maximum value of vibration parameter,  $x_{\min}$  is minimum value of vibration parameter,  $\Delta\tau$  is time interval,  $\phi$  is rotation angle of initial line,  $k$  is angle magnification factor, usually  $\phi = 60^\circ$ ,  $k = 20^\circ \sim 60^\circ$ ,  $\Delta\tau = 3 \sim 10$  [34]. Vibration parameters to be selected include amplitude, phase and so on, different parameters get different SPCI, this paper choose vibration amplitude.

**2) GLCM AND IMAGE FEATURE**

GLCM starts from pixel position  $(x, y)$  with gray level of  $i$ , and counts frequency  $P(i, j, d, \theta)$  that appears simultaneously with pixel position  $(x+D_x, y+D_y)$  of gray level  $j$  and

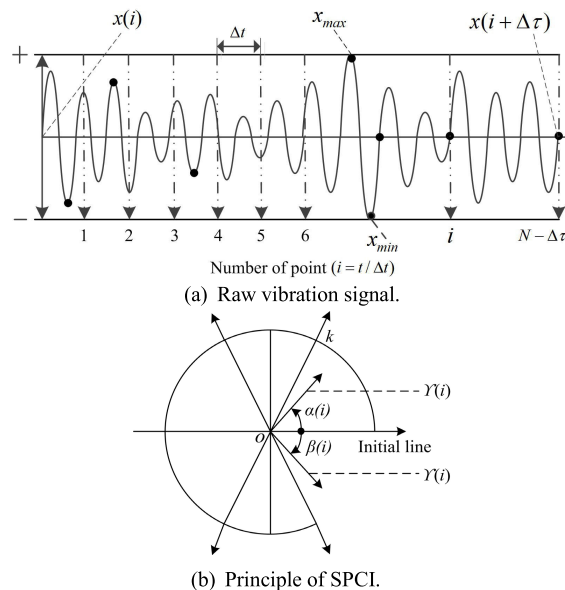


**FIGURE 7. Schematic diagram of SPCI.**

distance of  $d$ , and expression is

$$P(i, j, d, \theta) = \{[(x, y), (x+D_x, y+D_y)|f(x, y)=i, f(x+D_x, y+D_y)=j]\} \tag{27}$$

where  $i, j$  is gray level,  $i, j = 0, 1, 2, \dots, N-1$ ,  $D_x, D_y$  is position offset,  $d$  is generating step of GLCM,  $\theta$  is generating direction of GLCM, usually  $\theta = 0^\circ, 45^\circ, 90^\circ, 135^\circ$ , and finally an  $N \times N$  square matrix is obtained, as shown in Fig. 8.

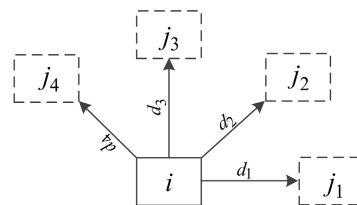


**FIGURE 8. Generating directions of GLCM.**

In order to extract image features, it is necessary to firstly do normalization as follows

$$g(i, j) = P(i, j) / \sum_{i=0}^{N-1} \sum_{j=0}^{N-1} P(i, j) \tag{28}$$

In this paper, maximum probability, entropy, contrast, correlation, energy, and inverse difference are taken as characteristic parameters of GLCM.

Maximum probability: maximum frequency of occurrence of gray pairs in GLCM.

$$mp = \max_{i,j} (g(i, j)) \tag{29}$$

Entropy: measurement of image content randomness, indicating complexity or inhomogeneity of texture. Entropy of

image is 0 when it has no texture, and maximum when it has full texture.

$$ent = - \sum_{i=0}^{N-1} \sum_{j=0}^{N-1} g(i, j) \log(g(i, j)) \quad (30)$$

Contrast: measurement of texture clarity, the deeper the furrow of image texture, the greater the contrast of image, the more obvious the texture effect, and vice versa.

$$con = \sum_{i=0}^{N-1} \sum_{j=0}^{N-1} (i - j)^2 g(i, j) \quad (31)$$

Correlation: measurement of grayscale linear relationship, measuring how similar elements of GLCM are in row or column directions.

$$cor = \sum_{i=0}^{N-1} \sum_{j=0}^{N-1} (i - \mu)(j - \mu) g(i, j) / \sigma^2 \quad (32)$$

where  $\mu = \sum_{i=0}^{N-1} \sum_{j=0}^{N-1} i \cdot g(i, j) / \sum_{i=0}^{N-1} \sum_{j=0}^{N-1} g(i, j)$ ,  $\sigma^2 = \sum_{i=0}^{N-1} \sum_{j=0}^{N-1} (i - \mu)^2 \cdot g(i, j)$ .

Energy: measurement of gray level change uniformity of image texture, reflecting degree of gray level distribution uniformity and degree of texture coarseness.

$$ene = \sum_{i=0}^{N-1} \sum_{j=0}^{N-1} g^2(i, j) \quad (33)$$

Inverse difference: measurement of local changes of image texture, reflecting homogeneity of image texture and representing regularity of texture. The more regular the texture, the larger the inverse moment, and vice versa.

$$idm = \sum_{i=0}^{N-1} \sum_{j=0}^{N-1} \left[ \frac{1}{1 + (i - j)^2} \right] g(i, j) \quad (34)$$

## V. TEST AND DISCUSSION

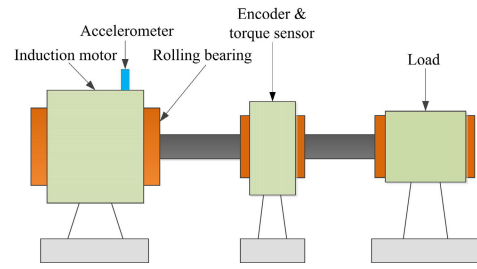
### A. TEST RIG AND VIBRATION DATA

In this paper, EMD-PWVD-FCM method is verified by vibration data of rolling bearing from Case Western Reserve University. Test rig is shown in Fig. 9.

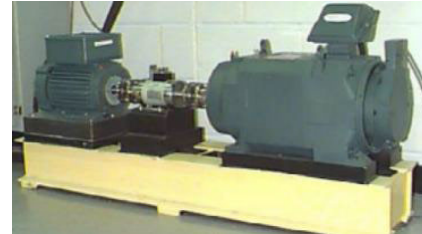
As shown in Fig. 9, test device is mainly composed of induction motor, encoder & torque sensor and load components. Fault position is at inner ring of rolling bearing, electrical discharge machining was used to fabricate ring defect of rolling bearing, and two kinds of fault diameter are 0.007 and 0.021 inches respectively. Accelerometer was used to collect vibration signals, selected signal sampling frequency is 12KHz, motor speed is 1797r/min.

### B. VERIFICATION SCHEME OF EMD-PWVD-FCM

In order to verify effectiveness of proposed EMD-PWVD-based FCM clustering method, it was compared with GI texture analysis-based and SPCI-based methods. Three kinds of vibration image method were used to transform and then extract features of rolling bearing vibration signals, and



(a) Scheme of test device.



(b) Actual test device.

FIGURE 9. Test rig.

FCM clustering was used to identify faults. Fault identification of original vibration signals and that of artificially noised signals with different signal-to-noise ratios (SNRs) were carried out respectively. Flowchart is shown in Fig. 10.

### C. RESULTS OF VIBRATION IMAGE TRANSFORM AND FEATURE EXTRACTION BY THREE METHODS

Time-domain waveform and frequency-domain spectrum of vibration signal under three different conditions are shown in Fig. 11. Fault degree can not be distinguished by directly reading the signal characteristic parameters from both time-domain and frequency-domain results, therefore vibration signals in Fig. 11 need to be transformed into vibration image, and transform results are shown in Table 2.

It can be seen from Table 2 that brightness of grayscale image increases gradually with aggravation of fault, petals of image generated by SPCI become thinner gradually, and gap between first pair of petals becomes larger when initial line is 0°, energy distribution of contour map generated by EMD-PWVD is changed. All three kinds of vibration images change with degree of fault, which provides foundation for image feature extraction and fault identification.

### D. IDENTIFICATION USING ORIGINAL SIGNALS

For original signal without artificially adding noise, 2048 sampling points were taken from each set of data and divided into 40 groups, of which 20 groups were used as training samples, 20 groups were used as test samples, for three cases altogether 60 groups of training samples and 60 groups of test samples, fault identification experiments by using three vibration image methods were carried out.

#### 1) GI ANALYSIS

Use LBP to analyze texture of the converted grayscale image, and then perform 2D-FT. Use Eq. (28) to calculate the square

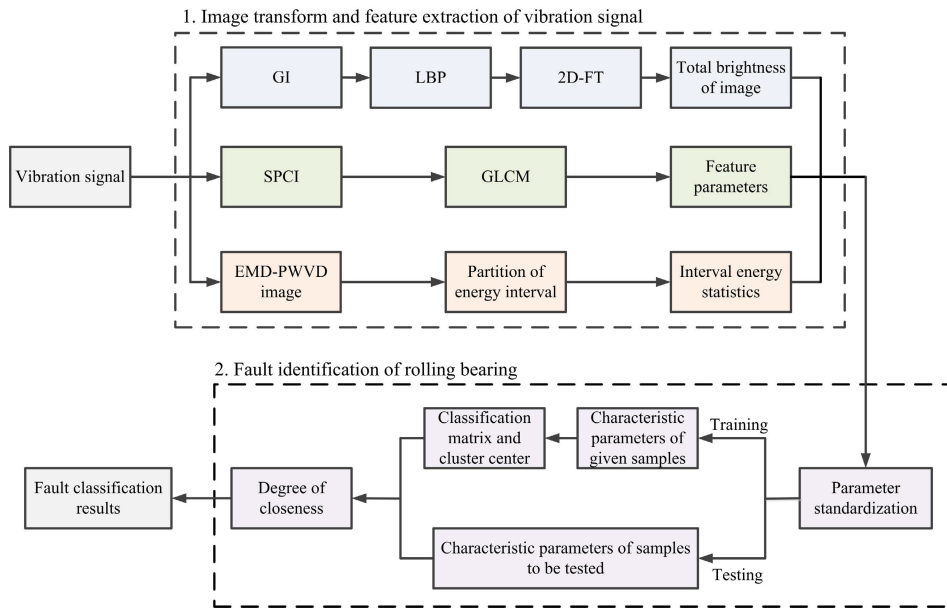


FIGURE 10. Flowchart of comparison study of three vibration image methods.

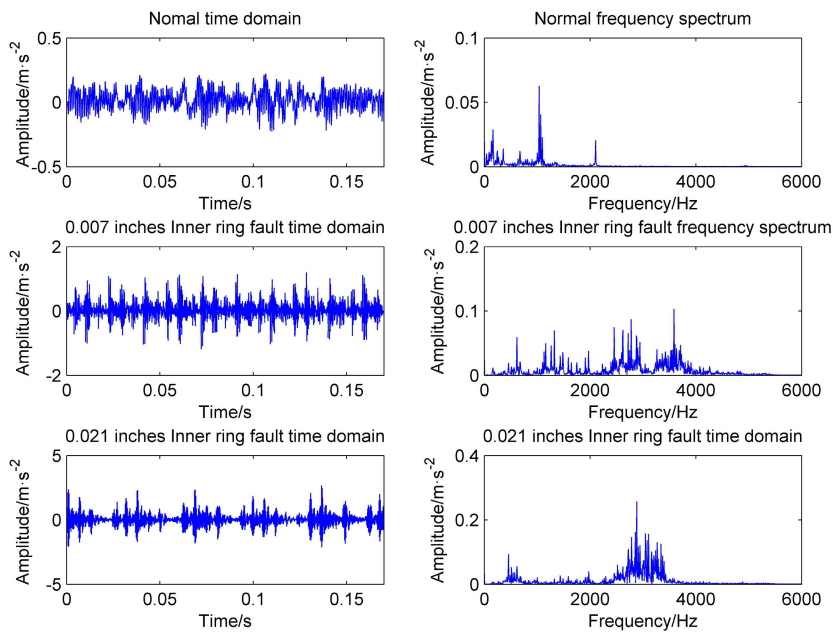


FIGURE 11. Time-domain waveform and frequency-domain spectrum of vibration signal under three cases.

sum  $E$  of 2D matrix value of image as characteristic parameter. Average value of each type of characteristic parameters of 60 sets of training samples were used as clustering center. Clustering center  $C$  is:

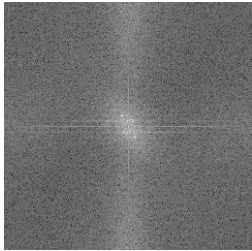
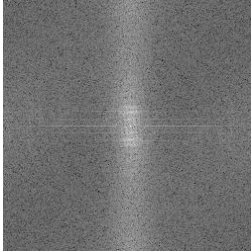
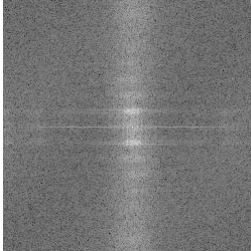
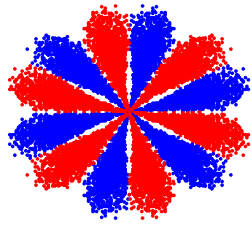
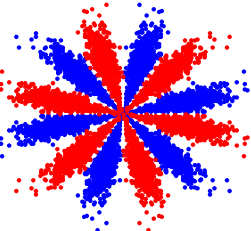
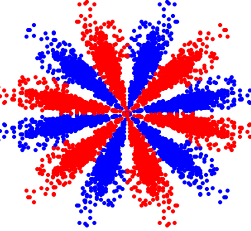
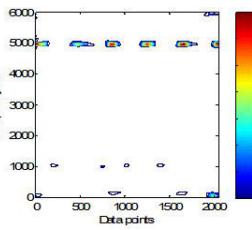
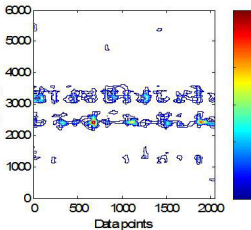
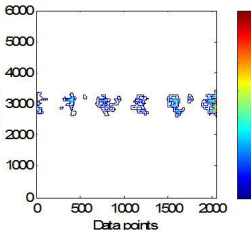
$$C = [585160.5586; 591687.5358; 597019.2929]$$

Clustering center  $C$  was used as a standard model for identifying inner ring faults of rolling bearing. Lines 1, 2, and 3 of  $C$  are clustering centers of sample data of normal

and defects of 0.007 and 0.021 inches, respectively. For 60 sets of unknown sample data, use Eq. (18) to calculate closeness to each line of standard mode  $C$ , and determine unknown fault category according to maximum closeness value. Perform fault identification on 45 groups of unknown samples, of which 9 groups of correct identification results are shown in Table 3. For 60 groups of classification, there is no omission beyond the obtained classification results. Through statistics, classification accuracy rate of 60 small



TABLE 2. Results of vibration image transformed by three methods.

Method	Normal	Inner ring fault diameter of 0.007 inches	Inner ring fault diameter of 0.021 inches
GI			
SPCI			
EMD-PWVD			

samples is 91.67%. This result proves that GI method can effectively identify inner ring faults of rolling bearing.

2) SPCI ANALYSIS

In order to study difference of vibration signal snowflake maps under different conditions, six characteristic parameters in four directions ( $\theta = 0^\circ, 45^\circ, 90^\circ, 135^\circ, d = 1$ ) of GLCM were extracted, and a total of 24 parameters were obtained. Because different directions contained different texture information, average of four directions was taken as GLCM during test. Six characteristic parameters were denoted as  $F_1$  to  $F_6$ ,  $F_1$  represents maximum probability,  $F_2$  represents entropy,  $F_3$  represents contrast,  $F_4$  represents correlation,  $F_5$  represents energy, and  $F_6$  represents inverse gap.

Normalize eigenvector matrix to get initial membership matrix:

$$x_{ij} = \frac{x_{ij} - \min(x_j)}{\max(x_j) - \min(x_j)} \tag{35}$$

where  $x_j$  is value of  $j$ -th column of matrix, denominator of Eq. (35) is difference between maximum and minimum values of elements in  $j$ -th column of original matrix. Data were compressed to [0,1] through standardization.

Characteristic parameters of 60 sets of training samples were standardized and used as FCM clustering input.

Set number of clusters to 3 and set iteration stop threshold to  $\varepsilon = 10^{-5}$ . After 6 iterations, membership matrix  $U$  of known samples was obtained. Clustering center  $C$  is:

$$C = \begin{bmatrix} 0.0482 & 0.1924 & 1.0000 & 0.0390 & 0.0000 & 0.0919 \\ 0.0658 & 0.0739 & 1.0000 & 0.0000 & 0.0077 & 0.1091 \\ 0.0970 & 0.0238 & 1.0000 & 0.0000 & 0.0354 & 0.1408 \end{bmatrix}$$

Identification step of this method is similar to that of GI. Finally, the unknown sample categories are determined by the maximum closeness value. Perform fault identification on 45 groups of unknown samples, of which 9 groups of correct identification results are shown in Table 4. For 60 groups of classification, there is no omission beyond the obtained classification results. Through statistics, classification accuracy rate of 60 small samples is 96.67%. This results prove that SPCI method can effectively identify inner ring faults of rolling bearing.

3) EMD-PWVD ANALYSIS

For EMD-PWVD method, energy distribution values in three frequency intervals under three states were used as characteristic parameters to distinguish different fault degrees of rolling bearing. Characteristic parameters of 60 sets of training samples were standardized and used as FCM clustering input. Set number of clusters to 3 and set iteration stop

TABLE 3. 9 groups of correct identification results by GI analysis.

Serial number	Accumulated energy ( $10^5$ )	Closeness			Identification result
		Normal	IR007	IR021	
1	5.868	<b>0.9872</b>	0.9668	0.8944	correct
2	5.858	<b>0.9983</b>	0.9427	0.8614	correct
3	5.863	<b>0.9951</b>	0.9572	0.8708	correct
4	5.940	0.9132	<b>0.9716</b>	0.9615	correct
5	5.914	0.9379	<b>0.9987</b>	0.9428	correct
6	5.924	0.9318	<b>0.9981</b>	0.9516	correct
7	5.974	0.8691	0.9546	<b>0.9926</b>	correct
8	5.958	0.8819	0.9612	<b>0.9754</b>	correct
9	5.971	0.8625	0.9431	<b>0.9985</b>	correct

TABLE 4. 9 groups of correct identification results by SPCI analysis.

Serial number	$F_1$	$F_2$	$F_3$	$F_4$	$F_5$	$F_6$	Closeness			Identification result
							Normal	IR007	IR021	
1	0.780	1.260	4.019	0.744	0.621	0.924	<b>0.9982</b>	0.9672	0.9437	correct
2	0.797	1.190	3.729	0.747	0.646	0.929	<b>0.9961</b>	0.9706	0.9471	correct
3	0.787	1.224	3.666	0.763	0.632	0.930	<b>0.9972</b>	0.9671	0.9437	correct
4	0.873	0.845	2.534	0.739	0.766	0.952	0.9599	<b>0.9933</b>	0.9833	correct
5	0.856	0.935	2.927	0.730	0.737	0.944	0.9739	<b>0.9927</b>	0.9693	correct
6	0.868	0.874	2.690	0.732	0.757	0.949	0.9647	<b>0.9981</b>	0.9785	correct
7	0.897	0.717	2.044	0.746	0.807	0.961	0.9239	0.94999	<b>0.9734</b>	correct
8	0.909	0.654	1.838	0.745	0.828	0.965	0.8808	0.9012	<b>0.9246</b>	correct
9	0.878	0.821	2.474	0.736	0.775	0.953	0.9547	0.9880	<b>0.9885</b>	correct

threshold to  $\varepsilon = 10^{-5}$ . After 4 iterations, membership matrix  $U$  of known samples was obtained. Clustering center  $C$  is:

$$C = \begin{bmatrix} 0.4128 & 0.0000 & 1.0000 \\ 0.0851 & 1.0000 & 0.0000 \\ 0.0000 & 1.0000 & 0.0390 \end{bmatrix}$$

Identification step of this method is similar to that of GI. Finally, the unknown sample categories are determined by the maximum closeness value. Fault identification results of 45 groups of unknown samples are shown in Fig. 12. It can be seen from Fig. 12 that three fault categories with different degrees are clearly distinguished, and 9 groups of correct identification results are given in Table 5. For 60 groups of classification, there is no omission beyond the obtained classification results. Through statistics,

classification accuracy rate of 60 samples is 90%, this results proves that EMD-PWVD method can effectively identify inner ring faults of rolling bearing.

**E. IDENTIFICATION USING ARTIFICIALLY NOISED SIGNALS**

In actual industrial field, vibration signal collected is usually polluted by strong background noise, field noise has great influence on signal processing and fault identification. In order to further verify robustness of this proposed method for actual noised signal, noises with different SNRs were artificially added to signals used above. SNR of vibration signal is defined as

$$SNR = 10 \log_{10} \left( \frac{P_s}{P_n} \right) \tag{36}$$

TABLE 5. 9 groups of correct identification results by EMD-PWVD method.

Serial number	0-2KHz accumulated energy	2-4KHz accumulated energy	4-6KHz accumulated energy	Closeness			Identification result
				Normal	IR007	IR021	
1	0.0017	2.3692E-05	0.0040	<b>0.9959</b>	0.2200	0.2046	correct
2	0.0016	2.7188E-05	0.0017	<b>0.8258</b>	0.0499	0.0345	correct
3	0.0022	2.9986E-05	0.0010	<b>0.6226</b>	0.2101	0.1947	correct
4	0.0200	0.0649	0.0137	0.2366	<b>0.9875</b>	0.9461	correct
5	0.0196	0.0579	0.0096	0.2647	<b>0.9594</b>	0.9181	correct
6	0.0164	0.0546	0.00861	0.2521	<b>0.9720</b>	0.9307	correct
7	0.0130	0.2523	0.0157	0.1996	0.9678	<b>0.9909</b>	correct
8	0.0086	0.1266	0.0098	0.1992	0.9682	<b>0.9904</b>	correct
9	0.0027	0.0998	0.0119	0.2272	0.9402	<b>0.9815</b>	correct

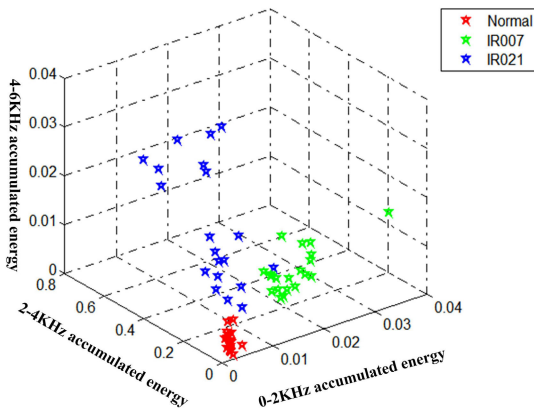


FIGURE 12. 3D clustering distribution diagram of EMD-PWVD method.

where  $p_s$  and  $p_n$  are power of signal and noise respectively. In this paper, Gaussian white noises with different SNRs were added, as shown in Fig. 13. In test, when SNR is 5, 10 and 15, identification was conducted under the same conditions as Part D, and identification results are shown in Table 6.

TABLE 6. Identification accuracy rate of three image methods under different SNRs.

Method	SNR=5	SNR=10	SNR=15	SNR=0	Maximum reduction
GI	63.33%	81.67%	88.33%	91.67%	28.34%
SPCI	65%	78.33%	96.67%	96.67%	31.67%
EMD-PWVD	75%	88.33%	93.33%	90%	15%

As can be seen from Table 6, identification accuracy rates of three methods are all over 90% under no added noise,

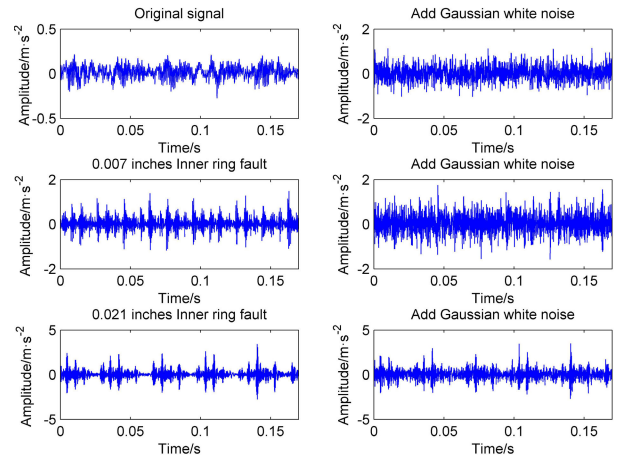


FIGURE 13. Original vibration signal and signal added Gaussian white noise in three cases when SNR is 10.

and SPCI reaches 96.67%, GI reaches 91.67%, EMD-PWVD reaches 90%. Of course, with different selection of feature indicators, recognition accuracy will change, and recognition accuracy of EMD-PWVD can be improved by dividing more energy intervals. With adding of noise and decrease of SNR, identification accuracy rates of SPCI and GI decrease rapidly. When SNR=5, SPCI reduced by 31.67%, GI reduced by 28.34%, while EMD-PWVD only reduced by 15%, which is about half those of other two methods. Therefore, it can be seen that EMD-PWVD method proposed in this paper is more suitable for signals with strong noise, its reason is that SPCI and GI methods do not process the collected vibration signals and then directly transform them into images, while EMD-PWVD method performs TFA on the collected

vibration signals to present clearly signal features. In industrial practice, all vibration signals contain background noise. Therefore, newly proposed EMD-PWVD method is optimal choice for actual industrial application.

## VI. CONCLUSION

Fault diagnosis of rolling bearing is an important research direction for reliability improvement of rotating machine. In this paper, EMD-PWVD-based vibration image transform and FCM clustering are integrated to realize intelligent fault diagnosis of rolling bearing.

(1) Vibration time-frequency image generation method by EMD-PWVD is proposed. This method can not only effectively solve the problem of cross-interference in the processing of complex signals, but also retain its excellent characteristics of time-frequency focusing.

(2) Fault diagnosis of rolling bearing is realized by using FCM clustering of EMD-PWVD vibration images. Firstly, vibration signal is transformed into contour time-frequency image by EMD-PWVD. Then, according to energy distribution of contour diagram, energy value at each interval is taken as characteristic parameter. Finally, combining FCM clustering, fault of inner ring for rolling bearing is identified by maximum closeness.

(3) Bearing data of Case Western Reserve University are used to verify the proposed method. Experimental results show that identification accuracy rate of EMD-PWVD-FCM reaches 90% by using three energy intervals under 60 groups of small samples. Compared with FCM clustering of GI and SPCI, when noise is added and SNR=5, identification accuracy of EMD-PWVD-FCM is reduced by only 15%, which is about half those of other two methods. Therefore, EMD-PWVD-FCM is effective and stable for noised vibration signals of rolling bearings in practice.

## REFERENCES

- [1] D. S. Shah and V. N. Patel, "A review of dynamic modeling and fault identifications methods for rolling element bearing," *Procedia Technol.*, vol. 14, pp. 447–456, Jan. 2014.
- [2] J. J. Zhang, Z. Q. Ma, M. Q. Wang, and W. Y. Ruan, "Rolling bearing fault feature extraction based on VMD and autocorrelation analysis," *J. Electron. Meas. Instrum.*, vol. 31, no. 9, pp. 1372–1378, Sep. 2017.
- [3] C. Yang, S. T. Yan, C. Z. He, G. D. Ma, and D. Q. Yuan, "Fault diagnosis of rolling bearings based on kurtosis and wavelet envelope analysis," *Machinery*, vol. 52, no. 2, pp. 62–64, Feb. 2014.
- [4] A. J. Hu, W. L. Ma, and G. J. Tang, "Rolling bearing fault feature extraction method based on ensemble empirical mode decomposition and kurtosis criterion," *Proc. CSEE*, vol. 32, no. 11, pp. 106–111, Apr. 2012.
- [5] X. T. Xie, S. B. Li, G. C. Yang, G. K. Liu, and X. M. Yao, "Fault diagnosis of rolling bearing based on FFT and CS-SVM," *Modular Mach. Tool Autom. Manuf. Techn.*, vol. 502, no. 4, pp. 95–99, Apr. 2019.
- [6] P. M. Baggenstoss and F. Kurth, "Comparing shift-autocorrelation with cepstrum for detection of burst pulses in impulsive noise," *J. Acoust. Soc. Amer.*, vol. 136, no. 4, pp. 1574–1582, Oct. 2014.
- [7] K. Chen, P. Fu, and H. Xie, "Application of cepstrum analysis in rolling bearing fault monitoring," *J. SiChuan Ordnance*, vol. 29, no. 1, pp. 93–96, Feb. 2018.
- [8] W. Sui, S. Osman, and W. Wang, "An adaptive envelope spectrum technique for bearing fault detection," *Meas. Sci. Technol.*, vol. 25, no. 9, Sep. 2014, Art. no. 095004.
- [9] X. Lou and K. A. Loparo, "Bearing fault diagnosis based on wavelet transform and fuzzy inference," *Mech. Syst. Signal Process.*, vol. 18, no. 5, pp. 1077–1095, Sep. 2004.
- [10] Z. K. Peng, P. W. Tse, and F. L. Chu, "A comparison study of improved Hilbert–Huang transform and wavelet transform: Application to fault diagnosis for rolling bearing," *Mech. Syst. Signal Process.*, vol. 19, no. 5, pp. 974–988, Mar. 2005.
- [11] N. E. Huang, Z. Shen, S. R. Long, M. C. Wu, H. H. Shih, Q. Zheng, N.-C. Yen, C. C. Tung, and H. H. Liu, "The empirical mode decomposition and the Hilbert spectrum for nonlinear and non-stationary time series analysis," *Proc. Roy. Soc. London A, Math., Phys. Eng. Sci.*, vol. 454, no. 1971, pp. 903–995, Mar. 1998.
- [12] R. Kumar and M. Singh, "Outer race defect width measurement in taper roller bearing using discrete wavelet transform of vibration signal," *Measurement*, vol. 46, no. 1, pp. 537–545, Jan. 2013.
- [13] Y. Y. Liu, K. Li, and P. Chen, "Fault diagnosis for rolling bearings based on synchro squeezing wavelet transform," *China Mech. Eng.*, vol. 29, no. 5, pp. 585–590, Mar. 2018.
- [14] T. Guo and Z. Deng, "An improved EMD method based on the multi-objective optimization and its application to fault feature extraction of rolling bearing," *Appl. Acoust.*, vol. 127, pp. 46–62, Dec. 2017.
- [15] M. Rezaee and A. T. Osguei, "Improving empirical mode decomposition for vibration signal analysis," *Arch. Proc. Inst. Mech. Eng., C J. Mech. Eng. Sci.*, vol. 231, no. 12, pp. 2223–2234, Feb. 2017.
- [16] B. Tang, W. Liu, and T. Song, "Wind turbine fault diagnosis based on Morlet wavelet transformation and Wigner–Ville distribution," *Renew. Energy*, vol. 35, no. 12, pp. 2862–2866, Dec. 2010.
- [17] Z. H. Yuan, M. Y. Xu, and X. X. Qi, "The certification for inevitability of cross-term in WVD," *Adv. Mater. Res.*, vols. 1030–1032, pp. 1930–1933, Sep. 2014.
- [18] Y. P. Cai, A. H. Li, T. Wang, L. Yao, and P. Xu, "Time-frequency analysis of internal combustion engine vibration based on EMD-Wigner–Ville," *J. Vib. Eng.*, vol. 23, no. 4, pp. 430–437, Aug. 2010.
- [19] W. J. Mu, L. S. Shi, Y. P. Cai, H. Liu, and G. Z. Jin, "IC engine fault diagnosis method based EMD-WVD and LNMf," *J. Vib. Shock*, vol. 35, no. 23, pp. 191–202, Dec. 2016.
- [20] T. O. Gulum, A. Y. Erdogan, K. K. Guner, L. Durak-Ata, T. Yildirim, and P. E. Pace, "PWVD resolution considerations for LFM CW signal detection by WHT," in *Proc. 20th Int. Conf. Microw., Radar Wireless Commun. (MIKON)*, Jun. 2014, pp. 1–4.
- [21] W. J. Mou, L. S. Shi, Y. P. Cai, G. Sun, and Y. Zheng, "IC engine fault diagnosis method based on KVMD-PWVD and LNMf," *J. Vib. Shock*, vol. 36, no. 2, pp. 45–51, Jan. 2017.
- [22] J. Uddin, R. Islam, J.-M. Kim, and C.-H. Kim, "A two-dimensional fault diagnosis model of induction motors using a Gabor filter on segmented images," *Int. J. Control Autom.*, vol. 9, no. 1, pp. 11–22, Jan. 2016.
- [23] X. Liu, Y. X. Jia, X. B. Su, and X. Zou, "Fault feature extraction for diesel engine misfires based on the gray image texture analysis," *J. Vib. Shock*, vol. 38, no. 2, pp. 145–150, Jan. 2019.
- [24] J. D. Jia, L. L. Zhang, H. H. Jiang, B. Zhou, Y. K. Xiao, and Z. K. Zhu, "A study on the wear fault diagnosis of transmission gears based on symmetric polar coordinates method," *Automot. Eng.*, vol. 35, no. 1, pp. 93–97, Jan. 2013.
- [25] C. Yang and T. Feng, "Abnormal noise diagnosis of internal combustion engine using wavelet spatial correlation filter and symmetrized dot pattern," *Appl. Mech. Mater.*, vol. 141, no. 1, pp. 168–173, Nov. 2011.
- [26] D.-T. Hoang and H.-J. Kang, "Rolling element bearing fault diagnosis using convolutional neural network and vibration image," *Cognit. Syst. Res.*, vol. 53, pp. 42–50, Jan. 2019.
- [27] J. Li, X. Yao, X. Wang, Q. Yu, and Y. Zhang, "Multiscale local features learning based on BP neural network for rolling bearing intelligent fault diagnosis," *Measurement*, vol. 153, Mar. 2020, Art. no. 107419.
- [28] X. L. Zhang, Q. Zhang, X. R. Qin, and Y. T. Sun, "Rolling bearing fault diagnosis based on ITD Lempel–Ziv complexity and PSO-SVM," *J. Vib. Shock*, vol. 35, no. 24, pp. 102–107, Dec. 2016.
- [29] X. Liu, L. Bo, and H. Luo, "Bearing faults diagnostics based on hybrid LS-SVM and EMD method," *Measurement*, vol. 59, pp. 145–166, Jan. 2015.
- [30] X. Zhang, X. L. Ni, J. M. Zhao, and F. C. Sun, "Rolling bearing fault diagnosis using modified K-means cluster analysis," *Vibroeng. Procedia*, vol. 10, pp. 155–166, Dec. 2016.
- [31] H. Li, W. Wang, P. Huang, and Q. Li, "Fault diagnosis of rolling bearing using symmetrized dot pattern and density-based clustering," *Measurement*, vol. 152, Feb. 2020, Art. no. 107293.

- [32] C. Zhou, X. Wu, C. Liu, and W. He, "Rolling bearing fault diagnosis based on EMD and fuzzy C means clustering," *J. KunMing Univ. Sci. Technol., Sci. Technol.*, vol. 34, no. 6, pp. 34–39, Dec. 2009.
- [33] J. C. Ren, L. L. Zhang, Y. K. Xiao, and Z. K. Zhu, "Diesel engine fault diagnosis based on symmetrical polar coordinate and image processing," *Vehicle Engine*, vol. 34, no. 6, pp. 86–91, Dec. 2013.
- [34] L. L. Zhang, J. C. Ren, H. J. Feng, Z. K. Zhu, and Y. K. Xiao, "Diagnosis of diesel engine crankshaft bearing fault based on symmetric polar coordinates and image recognition," *Chin. Internal Combustion Engine Eng.*, vol. 36, no. 4, pp. 144–149, Aug. 2015.
- [35] N. R. Pal and J. C. Bezdek, "On cluster validity for the fuzzy C-means mode," *IEEE Trans. Fuzzy Syst.*, vol. 3, no. 3, pp. 370–379, Sep. 1995.
- [36] W. Zhang and Y. K. Xiao, "Diagnosing crankshaft bearing fault based on the wavelet packet-fuzzy C mean clustering arithmetic," *J. Acad. Mil. Transp.*, vol. 11, no. 2, pp. 45–46, 2009.
- [37] L. Liu, S. Lao, P. W. Fieguth, Y. Guo, X. Wang, and M. Pietikäinen, "Median robust extended local binary pattern for texture classification," *IEEE Trans. Image Process.*, vol. 25, no. 3, pp. 1368–1381, Mar. 2016.
- [38] M. V. Noskov and V. S. Tutatchikov, "Modification of a two-dimensional fast Fourier transform algorithm by the analog of the Cooley–Tukey algorithm for a rectangular signal," *Pattern Recognit. Image Anal.*, vol. 25, no. 1, pp. 81–83, Jan. 2015.
- [39] H. W. Fan and S. J. Shao, "Unbalance fault diagnosis method of electric spindle based on gray image texture analysis," *Manuf. Technol. Mach. Tool*, no. 11, pp. 130–134, Nov. 2019.
- [40] H. W. Fan, S. J. Shao, X. H. Zhang, H. W. Ma, X. G. Cao, and M. Q. Jing, "A diagnosis method for unbalance fault of motorized spindles using symmetrical polar image and clustering of fuzzy C-means," *J. Xi'an Jiaotong Univ.*, vol. 53, no. 12, pp. 57–62, Dec. 2019.



**HONGWEI FAN** received the B.Sc. degree from Beihua University, in 2007, the M.Sc. degree from Northwestern Polytechnical University, in 2010, and the Ph.D. degree from Xi'an Jiaotong University, in 2015. He is currently a Lecturer with the School of Mechanical Engineering, Xi'an University of Science and Technology. His main research interests include intelligent monitoring, diagnosis, and control of equipment.



**SIJIE SHAO** was born in 1995. She received the B.Sc. degree from the Xi'an University of Science and Technology, in 2016, where she is currently pursuing the master's degree with the School of Mechanical Engineering. Her main research interest includes a vibration image fault diagnosis.



**XUHUI ZHANG** (Member, IEEE) received the B.Sc. and M.Sc. degrees from the Xi'an University of Science and Technology, in 1996 and 2002, respectively, and the Ph.D. degree from Xi'an Jiaotong University, in 2009. He is currently a Professor with the School of Mechanical Engineering, Xi'an University of Science and Technology. His main research interests include intelligent detection and control of equipment.



**XIANG WAN** received the B.Sc. degree from the China University of Geosciences, in 2005, and the Ph.D. degree from Xi'an Jiaotong University, in 2017. He is currently working with the Xi'an University of Science and Technology. His main research interests include machinery fault diagnosis and ultrasonic non-destructive testing.



**XIANGANG CAO** received the B.Sc. and M.Sc. degrees from the Xi'an University of Science and Technology, in 1994 and 1997, respectively, and the Ph.D. degree from Xi'an Jiaotong University, in 2008. He is currently a Professor with the School of Mechanical Engineering, Xi'an University of Science and Technology. His main research interest includes the condition monitoring of equipment.



**HONGWEI MA** received the B.Sc. and M.Sc. degrees from the Xi'an University of Science and Technology, in 1984 and 1993, and the Ph.D. degree from Xi'an Jiaotong University, in 1998. He is currently a Professor with the School of Mechanical Engineering, Xi'an University of Science and Technology. His main research interests include intelligent detection and control of equipment.

...